

Polytypism in xonotlite $\text{Ca}_6\text{Si}_6\text{O}_{17}(\text{OH})_2$

C. Hejny* and T. Armbruster*

Universität Bern, Laboratorium für chemische und mineralogische Kristallographie, Freiestr. 3, CH-3012 Bern, Switzerland

Received August 16, 1999; accepted January 3, 2001

Abstract. Occurrence, chemistry, crystal growth, technical applications, structure and polytypism of xonotlite $\text{Ca}_6\text{Si}_6\text{O}_{17}(\text{OH})_2$ are reviewed. Atomic coordinates of the three simplest ordered polytypes in modified Gard notation: *Ma2bc* (space group $P2_1/a$, $a = 17.032$, $b = 7.363$, $c = 7.012$ Å, $\beta = 90.36^\circ$), *Ma2b2c* (space group $A2/a$, $a = 17.032$, $b = 7.363$, $c = 14.023$, $\beta = 90.36^\circ$), and *M2a2bc* (space group $P\bar{1}$, $a = 8.712$, $b = 7.363$, $c = 7.012$ Å, $\alpha = 89.99^\circ$, $\beta = 90.36^\circ$, $\gamma = 102.18^\circ$) were modeled from geometric principles based on the known structure of the *M2a2b2c* polytype (space group $A\bar{1}$, $a = 8.712$, $b = 7.363$, $c = 14.023$, $\alpha = 89.99^\circ$, $\beta = 90.36^\circ$, $\gamma = 102.18^\circ$). Unique reflection arrangements in the reciprocal lattice, characteristic of each polytype, were defined as criteria to identify xonotlite polytypes on X-ray single-crystal photographs. Precession- and Weissenberg-photographs of a xonotlite from the Kalahari manganese field (Republic of South Africa) indicated the predominance of the (100) twinned *M2a2b2c* polytype, followed by the *Ma2b2c* polytype, and very low concentrations of the *Ma2bc* polytype. The *M2a2bc* polytype could not be identified which agrees with previous electron diffraction experiments on xonotlites from other localities. Diffuse streaks parallel to \mathbf{a}^* and less intensive ones parallel to \mathbf{c}^* on single-crystal photographs suggest the presence of additional disordered polytypes.

Introduction

The chemistry of phases composed of CaO, SiO₂ and H₂O is very complex and a large number of compounds is known in cement chemistry (Taylor, 1997). Due to their composition they are called C–S–H phases. Their crystallinity is rather poor and the stability of various phases is only loosely defined. Few crystal structures among the large number of possible C–S–H compounds have been solved. Prodan, Marinkovic, Vene, Kurbus and Boswell (1983) give an overview of known structures within the CaO–SiO₂–H₂O system.

Xonotlite $\text{Ca}_6[\text{Si}_6\text{O}_{17}](\text{OH})_2$ received its name from the type locality Tetela de Xonotla, Mexico (Rammelsberg,

1866). Eakleite was found to be identical with xonotlite (Larsen, 1923). Jurupaite was discredited and represents xonotlite with magnesium partly replacing calcium (Taylor, 1954).

In nature xonotlite occurs as vein forming mineral associated with other pure Ca-silicates as wollastonite, tobermorite, clinotobermorite, rosenhahnite and Ca-bearing silicates as pectolite, apophyllite, datolite, prehnite (Majer, Baric, 1971). Xonotlite is often a product of Ca-metasomatism and is then found at or close to a contact of calcium bearing rocks with igneous rocks. Many of the numerous deposits are associated with ultramafic bodies (Majer, Baric, 1971; O'Brien, Rodgers, 1973; Kaye, 1953; Smith, 1954). Other occurrences are in contact metamorphic limestone, as at the type locality, or in hornfelsed calc-silicate rock (Brown, 1978). Xonotlite dehydrates at 775–800 °C to wollastonite by an oriented transformation (Dent, Taylor, 1956).

Xonotlite has also technical applications; because of its stability at high temperature (<800 °C) it is a component of steam cured cements (Taylor, 1997). These cements are used for special applications such as fiber-reinforced materials of very low-density thermal insulation materials. Xonotlite in cementitious matrices, assessed for immobilization of radioactive waste, absorbs Cs from hydrous solutions (McCulloch, Angus, Crawford, Rahman, Glasser, 1985). Other applications of synthetic xonotlite comprise friction extender in brakepads of automobiles, pigment in paper and dye industry, thixotropic agent in paints, mortars, glues, dispersing and reinforcing agent in composites, flame retardant and drip suppressant in thermoplastics.

Xonotlite can be synthesized hydrothermally within few days at 200–350 °C and elevated pressure (Shirvastava, Komarneni, Breval, 1991; Yanagisawa, Feng, Yamasaki, 1997; Kalousek, Mitsuda, Taylor, 1977; Yanagisawa et al., 1997; Taylor, 1997; Stuckemeier, Dettmann, Mangold, Schweers, 1999). Xonotlite is believed to form topotactically out of tobermorite (Kalousek et al., 1977; Taylor, 1959). The crystallinity of synthetic xonotlite is of rather poor quality. ²⁹Si-NMR spectra of synthetic xonotlites showed an additional signal which was interpreted in terms of chain truncations whereas a corresponding signal was not observed in spectra of natural xonotlites of high crystallinity (Noma, Adachi, Matsuda, Yokoyama, 1998).

Several studies on both natural and synthetic xonotlites show higher water content than assumed by the formula

* Correspondence authors (e-mail: clivia.hejny@krist.unibe.ch, thomas.armbruster@krist.unibe.ch)

$\text{Ca}_6[\text{Si}_6\text{O}_{17}](\text{OH})_2$ (Grimmer, Wieker, 1971). In ^1H MAS NMR-spectra of synthetic and natural samples (Noma et al., 1998) the lines for structural CaOH and isolated SiOH could be deconvoluted. The spectrum consisted of a sharp and strong signal at 2.19 ppm assigned to structural CaOH (73% for the natural sample), a shoulder at 1.86 ppm interpreted as isolated SiOH (18% in the natural sample), and a broad signal at 5.26 ppm assigned to molecular H_2O (9% in the natural sample).

In xonotlite up to 5% of Si^{4+} may be substituted by Al^{3+} . These synthetic Al bearing specimens have cell parameters significantly different from Al free samples (Kalousek et al., 1977). The Ca/Si ratio is often found to be < 1 . To obtain charge balance in calcium deficient compositions additional protons have to be incorporated in the structure (Kalousek et al., 1977). Ca^{2+} can almost completely be substituted by Co^{2+} and Ni^{2+} (Komarneni, Roy, Roy, 1985) and partially be replaced by Mg^{2+} (Shrivastava, et al., 1991). Furthermore, low concentrations of Na^+ , K^+ , Mn^{2+} and Fe^{3+} are found in several natural xonotlite samples (deBruijn, Schoch, van der Westhuizen, Beukes, 1999).

The single-crystal diffraction pattern of xonotlite (Taylor, 1954; Kudoh, Takéuchi, 1979) shows sharp reflections, diffuse reflections and streaks. Considering only the sharp reflections a subcell was defined. Taking the streaks into account, a cell with doubled **b**-axis results. Sharp reflections are found for $k = 2n$, whereas the diffuse ones and streaks are observed for $k = 2n + 1$. The streaks run both parallel \mathbf{a}^* and \mathbf{c}^* , indicating one-dimensional disorder in two directions (Gard, 1966; Chisholm, 1980). Short spikes perpendicular to the above mentioned streaks, visible in electron diffraction images, have been interpreted in terms of two-dimensional disorder (Dornberger-Schiff, 1964).

Mamedov and Belov (1955, 1956a) were the first to propose a structure model for xonotlite (later confirmed by Eberhard, Hamid, Röttger, 1981). The structure consists of calcium polyhedral layers and infinite SiO_4 double chains. Based on this structure model, six polytypes, four ordered and two one-dimensionally disordered, were suggested and their corresponding reciprocal lattices were illustrated (Gard, 1966). Furthermore, five of these polytypes were confirmed by electron diffraction on natural samples (Gard, 1966; Chisholm, 1980). The first complete structure determination of an ordered polytype, previously predicted by Gard (1966), has been carried out by Kudoh and Takéuchi (1979).

The experimental objective of the present study is to identify xonotlite polytypes from single-crystal diffraction patterns. There has been no example reported as yet where a macroscopic xonotlite crystal was only composed of one polytype without additional disorder. In general, crystals represent polytypic intergrowths with additional twinning and disorder as evidenced by streaking in single-crystal X-ray or electron diffraction patterns. For a successful identification of the various ordered polytypes, their structures must be known in order to calculate the diffraction pattern in various crystallographic orientations. Two methods may be applied for modeling ordered xonotlite polytypes: (1) Derivation from strictly geometric principles, where a

structural module, derived from a known xonotlite polytype, is defined. This module is subsequently stacked to yield various polytype structures predicted and observed by Gard (1966). (2) Derivation by OD-theory (Dornberger-Schiff, 1956, 1964), which is based on application of special symmetry operations on a specific layer, the so called partial symmetry operations (σ operation). Both methods lead to corresponding results. In this study we have chosen the simple geometric approach because it does not require knowledge of OD-theory. Nevertheless, the OD-character will be discussed in a separate section.

Structure and polytypism

The basic structural features

Common to all polytypes is a polyhedral layer of one calcium atom in octahedral and two calcium atoms in sevenfold coordination (Fig. 1). The calcium atoms in sevenfold coordination have six close neighbors in form of a trigonal prism plus a seventh oxygen attached at one prism face. The octahedra are edge-sharing to form an infinite chain along the **b**-axis (chain A). A corresponding chain of edge-sharing polyhedra along the **b**-axis is built by the calcium atoms in sevenfold coordination (chains B and B'). All chains are joined together by edge-sharing to form a layer parallel (001) with a BAB'-arrangement of the chains. Chain B and B' are related to each other by a two-fold axis parallel to **b** and a mirror plane perpendicular to it. Thus the arrangement of only Ca-oxygen polyhedra in xonotlite can be described in a cell with $a = 17.031$, $b = 3.682$, $c = 7.012$ Å, $\beta = 90.37^\circ$ of $C2/m$ symmetry (Kudoh, Takéuchi, 1979).

The Ca polyhedral layers are linked by $[\text{Si}_6\text{O}_{17}]$ -double chains. Each $[\text{Si}_6\text{O}_{17}]$ -double chain (Fig. 2) consists of a

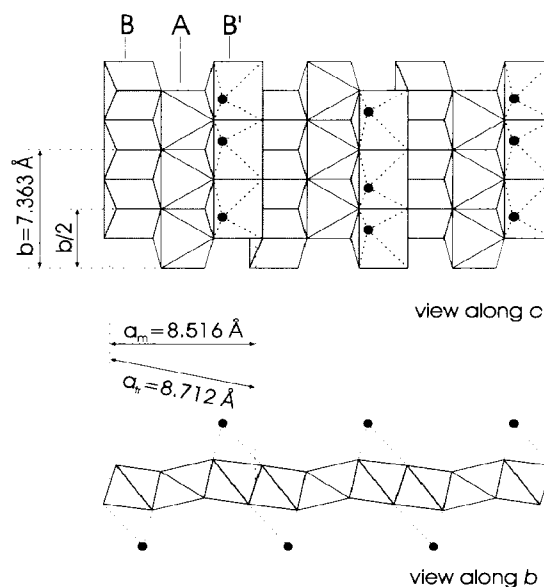


Fig. 1. Calcium polyhedral layer in the structure of xonotlite. Chains of calcium atoms in octahedral coordination, type A, are light gray. Chains of calcium atoms in seven-fold coordination, type B, B', are dark gray. The sevenfold coordination sphere is composed of a trigonal prism plus an additional seventh oxygen atom (black dots).

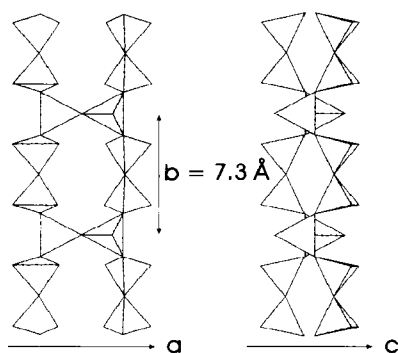


Fig. 2. $[\text{Si}_6\text{O}_{17}]$ -'Dreier-doppelkette' in xonotlite seen along the c -axis (left) and along the a -axis (right). b vertical.

wollastonite-like pair of $[\text{Si}_3\text{O}_9]$ -'Dreier-einfachketten' of corner-linked SiO_4 tetrahedra. This single chain has a periodicity of three tetrahedra, two of them are joined to give a $[\text{Si}_2\text{O}_7]$ -pair alternating with a single tetrahedron which connects the paired tetrahedra and is therefore labeled bridging tetrahedron. In xonotlite two $[\text{Si}_3\text{O}_9]$ -'Dreier-einfachketten' are joined to form a $[\text{Si}_6\text{O}_{17}]$ -'Dreier-doppelkette' by sharing apical oxygen atoms of two bridging tetrahedra. The two single chains are related to each other by an inversion center, a two-fold axis, and a mirror plane perpendicular to the two-fold axis, thus the symmetry of the double chain is $2/m$.

The OH group is located at the free apices of calcium octahedra where no bridging SiO_4 tetrahedra are attached. OH stretching frequencies at 3636 cm^{-1} indicate that the $\text{O}-\text{H}\cdots\text{O}$ distance is rather long, ca 3.3 \AA (Kalousek, Roy, 1957; Libowitzky, 1999). Protons associated with SiO_4 tetrahedra (silanol groups) as derived from ^1H MAS NMR spectroscopy (Noma et al., 1998) have not been located in the structure so far. Surplus H_2O molecules are assumed in the centers of the eight-membered rings of the double chains (Kudoh, Takéuchi, 1979).

Polytypes explained as different stacking of a protoxonotlite cell

Due to the fact that the $[\text{Si}_6\text{O}_{17}]$ -'Dreier-doppelkette' has the same length as two calcium polyhedra, each double chain of SiO_4 -tetrahedra can be attached to the calcium octahedra at two different positions (Fig. 3). This is the reason for the appearance of the various polytypes.

To visualize and compare the polytypes, a small unit common to both polytype structures (Mamedov, Belov, 1955, 1956a; Kudoh, Takéuchi, 1979) was introduced. This common unit has monoclinic symmetry, it is named 'cell of hypothetical protoxonotlite' (Kudoh, Takéuchi, 1979) and has dimensions of: $a_p = 8.516$, $b_p = 7.363$, $c_p = 7.012\text{ \AA}$, $\beta_p = 90.37^\circ$. Polytype structures may be explained as different arrangements of this protoxonotlite cell. Note that this protoxonotlite cell (dotted line in Figs. 4, 5 and 6) is not a crystallographically correct unit cell. This is because the protoxonotlite cell does not comply with the requirement of three-dimensional periodic translation, but it is necessary that along $[100]$ adjacent cells are shifted by $\pm b/4$ or $-\text{b}/4$. Neither the calcium

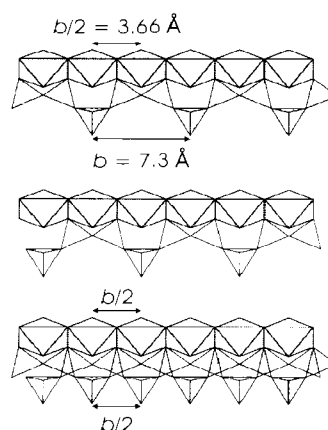


Fig. 3. Two possibilities of connecting a chain of SiO_4 tetrahedra with a periodicity of three tetrahedra to a column of calcium octahedra (type A) in xonotlite (top and middle) and column of calcium octahedra with two superimposed SiO_4 chains (bottom).

ribbon nor the next double chain of SiO_4 tetrahedra can be correctly placed without this $\pm b/4$ shift. In addition, along $[001]$ adjacent protoxonotlite cells are either juxtaposed or shifted by $b/2$. Only along $[010]$ the protoxonotlite cell is always repeated by normal translation. According to this

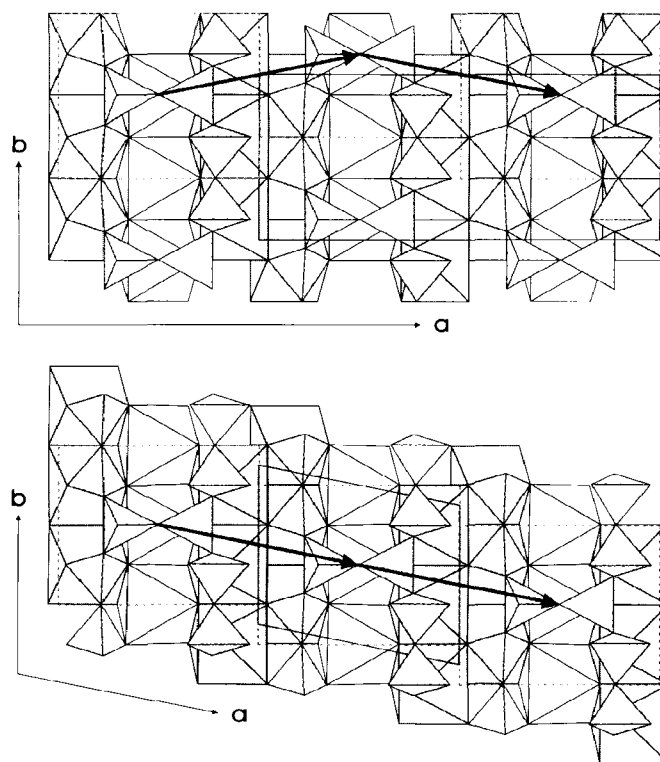


Fig. 4. Difference between two reported polytypes of xonotlite in a view along $[001]$. Top: xonotlite polytype as proposed by Mamedov and Belov (1955). In a -direction adjacent protoxonotlite cells are shifted (arrows) alternately by $+\text{b}/4$ and $-\text{b}/4$. Bottom: xonotlite polytype refined by Kudoh and Takéuchi (1979). In a -direction adjacent protoxonotlite cells are shifted (arrows) continuously by $+\text{b}/4$ (or $-\text{b}/4$). SiO_4 tetrahedra are patterned, calcium octahedra light gray, calcium polyhedra in seven-fold coordination dark gray. Protoxonotlite cells (Kudoh and Takéuchi, 1979) have dotted lines.

approach, the first difference between the monoclinic polytype (Mamedov, Belov, 1955, 1956a) and the triclinic one (Kudoh, Takéuchi, 1979) is the repetition of protoxonotlite cells along [100] (Fig. 4). In the monoclinic structure (Mamedov, Belov, 1955, 1956a) the protoxonotlite cells are alternately shifted by $+b/4$ and $-b/4$, whereas in the triclinic polytype (Kudoh, Takéuchi, 1979) they are arranged by a continuous step of $+b/4$ (or $-b/4$). A second difference occurs parallel to the c -axis (Fig. 5). In the monoclinic polytype the tetrahedral double chains are juxtaposed whereas in the triclinic polytype adjacent protoxonotlite cells are shifted by $b/2$. This structure description already suggests that xonotlite may exhibit one-dimensional disorder parallel to the a - and c -direction and hence polytypes distinct in stacking along both directions. The predicted disorder is confirmed by the presence of streaks along a^* and c^* in single-crystal X-ray and electron diffraction patterns (Kudoh, Takéuchi, 1979; Gard, 1966; Chisholm, 1980).

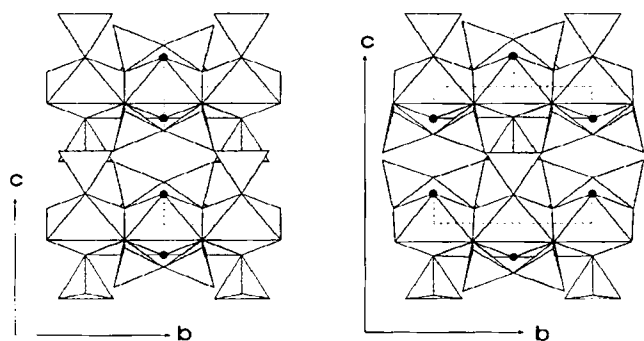


Fig. 5. Difference between two reported polytypes of xonotlite in a view along [100]. Left: xonotlite polytype as proposed by Mamedov and Belov (1955). Protoxonotlite cells are periodically repeated parallel to c . Right: xonotlite polytype refined by Kudoh and Takéuchi (1979). Protoxonotlite cells are shifted by $b/2$. Black circles are OH-position; color-codes as in Fig. 4. Notice that in the Mamedov and Belov (1955) polytype, Ca octahedra with two OH groups alternate with non-hydroxylated Ca octahedra. In contrast, in the Kudoh and Takéuchi (1979) polytype each Ca octahedron carries one OH group.

The Gard notation of xonotlite polytypes

Gard (1966) proposed a system of nomenclature for xonotlite and other fibrous calcium silicates. He derived this system in reciprocal space only by referring to a subcell¹ determined from sharp reflections (also named family reflections) characteristic of a polytype family. The arrangement of these sharp reflections in reciprocal space corresponds to the periodic arrangement of Ca-oxygen coordination polyhedra in direct space. Relating the size of this subcell to lattice parameters of an individual polytype, a four-digit suffix LUVW was obtained. L is the Bravais lattice type of the specified polytype in a setting with the crystal axes parallel to the subcell. The numbers UVW denote multiples of the subcell leading to following equations. In reciprocal space: $U \cdot a_{\text{polytype}}^* = a_{\text{subcell}}^*$, $V \cdot b_{\text{polytype}}^* = b_{\text{subcell}}^*$, $W \cdot c_{\text{polytype}}^* = c_{\text{subcell}}^*$; in direct space: $a_{\text{polytype}} = U \cdot a_{\text{subcell}}$, $b_{\text{polytype}} = V \cdot b_{\text{subcell}}$, $c_{\text{polytype}} = W \cdot c_{\text{subcell}}$.

Gard (1966) obviously used the pseudo-orthorhombic subcell proposed by Mamedov and Belov (1955, 1956a) for xonotlite: $a = 16.53$, $b = 3.637$, $c = 7.04$ Å, $\alpha = \beta = \gamma = 90^\circ$ of monoclinic symmetry $C12/m1$ (numerical values are not provided by Gard). This cell is equivalent to the revised cell given by Kudoh and Takéuchi (1979) with $a = 17.031$, $b = 3.682$, $c = 7.012$ Å, $\beta = 90.37^\circ$ of $C2/m$ symmetry describing the arrangement of Ca coordination polyhedra. In Gard's notation the monoclinic polytype of Mamedov and Belov (1955, 1956a) is named P121, whereas the triclinic polytype of Kudoh and Takéuchi (1979) is named F222. If this F222 setting is Niggli reduced a corresponding triclinic cell of $A\bar{1}$ space group symmetry is derived (Fig. 6).

¹ SUBCELL: Also named PSEUDOCCELL in older literature (e.g. Gard, 1966; Taylor, 1954). If a subcell is derived from sharp family reflections in terms of OD-theory (Dornberger-Schiff, 1956, 1964; Merlino, 1997) it is called family cell.

PROTOXONOTLITE CELL according to Kudoh, Takéuchi (1979): Small structural unit common to all polytypes; different polytypes are derived by different stacking of this protoxonotlite cell. A protoxonotlite cell is not necessarily a unit cell in conventional crystallographic meaning.

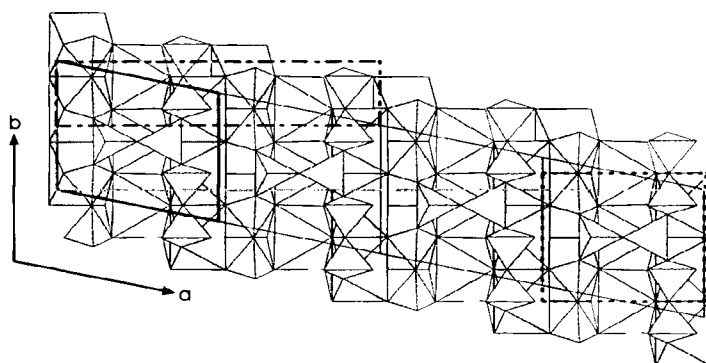


Fig. 6. Triclinic xonotlite $M2a2b2c$ polytype in its triclinic (Kudoh and Takéuchi, 1979) and pseudo-orthorhombic setting (labeled F222 by Gard, 1966). In addition, the protoxonotlite cell, and the subcell are given.

— full line: cell of triclinic xonotlite (Kudoh and Takéuchi, 1979)
 - - - - - dashed line: F222 cell (Gard, 1966)
 ······ dotted line: protoxonotlite cell (Kudoh and Takéuchi, 1979)
 - · - · - dashed-dotted line: xonotlite subcell

A modified Gard notation was approved by the International Union of Crystallography (Guinier, Bokij, Boll-Dornberger, Cowley, Đurovič, Jagodzinski, Krishna, De-Wolff, Zvyagin, Cox, Goodman, Hahn, Kuchitsu, Abrahams, 1984) where the first letter indicates the monoclinic system of the subcell (M). Three lower-case letters, accompanied by numbers if necessary, follow the symmetry symbol to indicate the periodicity along the three axes. In order to distinguish the ordered and disordered polytypes, an additional symbol d (abbreviation for disordered) is added as a subscript to the letter involved. In the following we use this modified Gard notation. For clarity we will sometimes additionally refer to the Gard (1966) notation given in parentheses.

Four simplest ordered polytypes

As already mentioned in the description of the xonotlite structure variable stacking occurs in two directions. In \mathbf{a} -direction adjacent protoxonotlite cells are shifted either by $+\mathbf{b}/4$ or $-\mathbf{b}/4$ leading to the two possibilities of either continuous shift by $+\mathbf{b}/4$ (or $-\mathbf{b}/4$) or alternating shift by $-\mathbf{b}/4$ and $+\mathbf{b}/4$. In \mathbf{c} -direction adjacent protoxonotlite cells are either juxtaposed or shifted by $+\mathbf{b}/2$. Combining

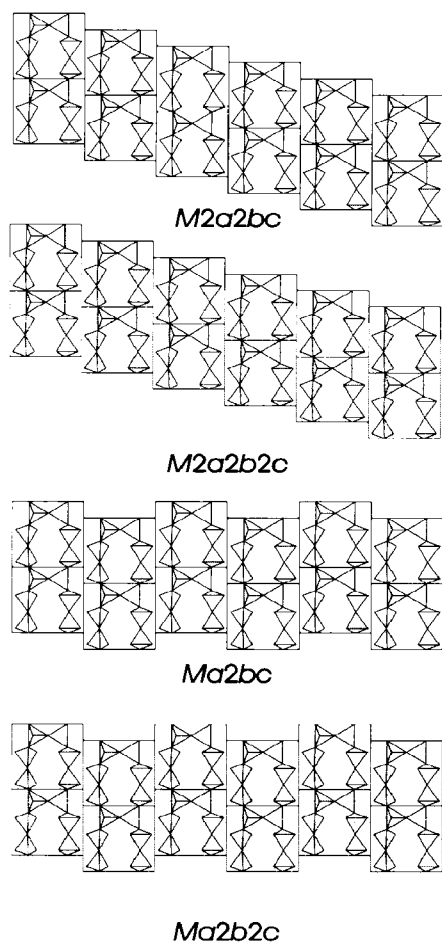


Fig. 7. Arrangement of protoxonotlite cells and double chains of SiO_2 tetrahedra in the four ordered xonotlite polytypes projected parallel \mathbf{c} , \mathbf{b} vertical, \mathbf{a} horizontal. Labeling of the polytypes according to the modified Gard nomenclature (Guinier et al. 1984).

the different stacking mechanisms in both directions, the following four simplest ordered polytypes result (Fig. 7). The term 'simplest polytypes' means, that more sophisticated combinations, such as $(+\mathbf{b}/4, +\mathbf{b}/4, -\mathbf{b}/4)$ or $(+\mathbf{b}/4, +\mathbf{b}/4, -\mathbf{b}/4, -\mathbf{b}/4)$..., for along \mathbf{a} adjacent protoxonotlite cells or combinations as (no shift, shift of $\mathbf{b}/2$) or (shift of $\mathbf{b}/2$, shift of $\mathbf{b}/2$, no shift) ... for along \mathbf{c} adjacent protoxonotlite cells are not considered.

$M2a2bc$ (C221): continuous shift of protoxonotlite cells by $+\mathbf{b}/4$ for stacking in \mathbf{a} -direction and juxtaposed cells along [001].

$M2a2b2c$ (F222): continuous shift of protoxonotlite cells by $+\mathbf{b}/4$ for stacking in \mathbf{a} -direction and shift of $+\mathbf{b}/2$ for stacking in \mathbf{c} -direction. This arrangement leads to the triclinic polytype as refined by Kudoh and Takéuchi (1979).

$Ma2bc$ (P121): alternate shift of protoxonotlite cells by $+\mathbf{b}/4$ and $-\mathbf{b}/4$ for stacking in \mathbf{a} -direction and juxtaposed cells along [001]. This arrangement leads to the monoclinic polytype as proposed by Mamedov and Belov (1955, 1956a).

$Ma2b2c$ (A122): alternate shift of protoxonotlite cells by $+\mathbf{b}/4$ and $-\mathbf{b}/4$ for stacking in \mathbf{a} -direction and shift by $+\mathbf{b}/2$ for stacking in \mathbf{c} -direction.

For $M2a2bc$ and $M2a2b2c$ a continuous shift of protoxonotlite cells by $-\mathbf{b}/4$ for stacking in \mathbf{a} -direction is just as possible as the shift by $+\mathbf{b}/4$ introduced above. Domains with only $-\mathbf{b}/4$ and domains with only $+\mathbf{b}/4$ shifts are in a twin relationship. The composition plane between the two twin components is (100) and a two-fold rotation about \mathbf{b} is the twin operation. If both twin sectors are evident on diffraction photographs we will call these polytypes $M2a2bc$ -twin and $M2a2b2c$ -twin.

Disordered polytypes

Gard (1966) originally proposed the two disordered polytypes $P \times 21$ and $A \times 22$ which become in the modified notation Ma_d2bc and Ma_d2b2c . Notice that in direct space these disordered polytypes are closely related to $M2a2bc$ -twin and $M2a2b2c$ -twin with the difference that in the disordered polytypes the domains are so small that in the diffraction pattern streaks are observed parallel to \mathbf{a}^* . Gard (1966) did not observe streaking parallel to \mathbf{c}^* but such streaks were recorded by Chisholm (1988). Thus, the Gard system may be extended by additional polytypes $Ma2bc_d$ and $Ma2b2c_d$. In direct space these polytypes describe disorder where protoxonotlite cells are either juxtaposed along [001] or shifted by $\mathbf{b}/2$. Even disorder in two directions may be expected which would lead to the Ma_d2bc_d polytype.

Modeling and identification of polytypes

Modeling of the four simplest ordered polytypes

One of the aims of this study was to model the structures and diffraction patterns of the four simplest ordered polytypes and to find an easy way to distinguish them. The protoxonotlite cell (Kudoh, Takéuchi, 1979) is a very good

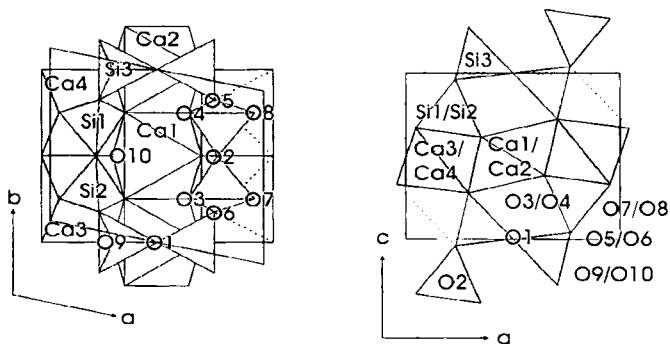


Fig. 8. Labeling of the atoms in the $M2a2bc$ polytype of xonotlite. Atoms in other polytypes are correspondingly labeled.

model to understand how the different polytypes look like, but to calculate a diffraction pattern conventional structure models are needed.

The refined structure of the $M2a2b2c$ polytype (Kudoh, Takéuchi, 1979) was taken as basic structure to calculate the structures of the three other simplest polytypes. The cell dimensions of the $M2a2bc$ polytype were obtained by halving the c -lattice parameter of the $M2a2b2c$ polytype (Kudoh, Takéuchi, 1979), leading to $a = 8.712$, $b = 7.363$, $c = 7.012$ Å. $\alpha = 89.99$, $\beta = 90.36$, $\gamma = 102.18^\circ$. Because of $\gamma \neq 90^\circ$ a three dimensional periodic arrangement of this cell gives a crystallographically correct structure (Fig. 8) and shifts by $+b/4$ along a , like in the model of the protoxonotlite cell, are already implied in the triclinic angle of $\gamma = 102.18^\circ$. Only half of the atoms in the structure Kudoh and Takéuchi (1979) are required for the structure of the $M2a2bc$ polytype, that is two calcium octahedra, four seven-coordinated calcium polyhedra and one unit of the Si_6O_{17} double chain. The corresponding atoms

were transformed with $\begin{pmatrix} 1 & 0 & 0 \\ 0 & 1 & 0 \\ 0 & 0 & 2 \end{pmatrix}$ into the new cell.

$M2a2bc$ -twin and $M2a2b2c$ -twin were obtained by transforming the cell of the respective polytype with

$$\begin{pmatrix} 1 & 0.5 & 0 \\ 0 & 1 & 0 \\ 0 & 0 & 1 \end{pmatrix}.$$

For the calculation of the $Ma2bc$ polytype, the cell of the former modeled $M2a2bc$ polytype was quadrupled along a . The first set of atoms was obtained by transforming the atoms of the $M2a2bc$ polytype by $x/4, y, z$. The second set was calculated by addition of $x + 0.25, y, z$ the third by addition of $x + 0.5, y + 0.5, z$ and the fourth set by addition of $x + 0.75, y + 0.5, z$.

Table 1. Lattice parameter and true symmetry of the ordered xonotlite polytypes. M is the matrix to transform the given setting into the

Polytype	a [Å]	b [Å]	c [Å]	α [°]	β [°]	γ [°]	SG	Z	M
$M2a2bc^a$	8.712	7.363	7.012	89.99	90.36	102.18	$P\bar{1}$	1	410/010/002
$M2a2b2c^a$	8.712	7.363	14.023	89.99	90.36	102.18	$A\bar{1}$	2	410/010/001
$Ma2bc$	17.032	7.363	7.012	90.0	90.36	90.0	$P2/a$	2	200/010/002
$Ma2b2c$	17.032	7.363	14.023	90.0	90.36	90.0	$A2/a$	4	200/010/001

a: twin component I

Table 2. Atomic coordinates of the $M2a2bc$ xonotlite polytype. $a = 8.712$, $b = 7.363$, $c = 7.012$ Å, $\alpha = 89.99$, $\beta = 90.36$, $\gamma = 102.18^\circ$, $P1$.

Atom	x	y	z
Ca1	0.5000	0.5000	0.5000
Ca2	0.5000	0.0000	0.5000
Ca3	0.1335	0.1645	0.3368
Ca4	0.1385	0.6537	0.3414
Si1	0.2118	0.2170	0.7682
Si2	0.2118	0.6389	0.7686
Si3	0.3182	0.9547	0.0562
O1	0.5000	0.0000	0.0000
O2	0.2190	0.4303	0.8422
O3	0.3512	0.7179	0.6192
O4	0.3434	0.2059	0.6174
O5	0.2297	0.1116	0.9720
O6	0.2294	0.7538	0.9716
O7	0.0424	0.6382	0.6652
O8	0.0463	0.1339	0.6740
O9	0.2988	0.9506	0.2780
O10	0.2977	0.4481	0.2694

Table 3. Atomic coordinates of the $M2a2b2c$ xonotlite polytype. $a = 8.712$, $b = 7.363$, $c = 14.023$ Å, $\alpha = 89.99$, $\beta = 90.36$, $\gamma = 102.18^\circ$, $A1$ (Kudoh and Takéuchi, 1979).

Atom	x	y	z
Ca1	0.5046	0.0016	0.7523
Ca3	0.1335	0.1645	0.6684
Ca4	0.1385	0.6537	0.6707
Si1	0.2118	0.2170	0.3841
Si2	0.2118	0.6389	0.3843
Si3	0.3182	0.9547	0.5281
O1	0.5000	0.0000	0.0000
O2	0.2190	0.4303	0.4211
O3	0.3512	0.7179	0.3096
O4	0.3434	0.2059	0.3087
O5	0.2297	0.1116	0.4860
O6	0.2294	0.7538	0.4858
O7	0.0424	0.6382	0.3326
O8	0.0463	0.1339	0.3370
O9	0.2988	0.9506	0.6390
O10	0.2977	0.4481	0.6347

The $Ma2b2c$ polytype was modeled similar as the $Ma2bc$ polytype, but directly out of the $M2a2b2c$ polytype (Kudoh, Takéuchi, 1979).

In general, atomic coordinates were calculated for a hypothetical structure of space group $P1$. The structure factors $F(hkl)$ of the four predicted structures were calculated for all reflections up to $42.5^\circ \theta$ using the program FCGEN (1998) with neutral-atom scattering factors for $\text{MoK}\alpha_1$ -radiation. Based on extinction rules for F_{calc}^2 in the reciprocal lattice a Niggli reduced cell and the true symmetry was subsequently determined for all polytypes

common setting of $a = 34.064$, $b = 7.363$, $c = 14.023$ Å, $\alpha = \gamma = 90$, $\beta = 90.36^\circ$. SG is the space group.

Table 4. Atomic coordinates of the *Ma2bc* xonotlite polytype, $a = 17.032$, $b = 7.363$, $c = 7.012$ Å, $\alpha = \gamma = 90^\circ$, $\beta = 90.36^\circ$, $P2_1/a$.

Atom	<i>x</i>	<i>y</i>	<i>z</i>
Ca1	0.2500	0.3750	0.5000
Ca2	0.2500	0.8750	0.5000
Ca3	0.0668	0.1311	0.3368
Ca4	0.0693	0.6191	0.3414
Si1	0.1059	0.1641	0.7682
Si2	0.1059	0.5860	0.7686
Si3	0.1591	0.8752	0.0562
O1	0.2500	0.8750	0.0000
O2	0.1095	0.3756	0.8422
O3	0.1756	0.6301	0.6192
O4	0.1717	0.1201	0.6174
O5	0.1149	0.0542	0.9720
O6	0.1147	0.6965	0.9716
O7	0.0212	0.6276	0.6652
O8	0.0215	0.1223	0.6740
O9	0.1494	0.8759	0.2780
O10	0.1489	0.3737	0.2694

Table 5. Atomic coordinates of the *Ma2b2c* xonotlite polytype, $a = 17.032$, $b = 7.363$, $c = 14.023$ Å, $\alpha = \gamma = 90^\circ$, $\beta = 90.36^\circ$, $A2/a$.

Atom	<i>x</i>	<i>y</i>	<i>z</i>
Ca1	0.2730	0.8755	0.7523
Ca3	0.0668	0.1311	0.6684
Ca4	0.0693	0.6191	0.6707
Si1	0.1059	0.1641	0.3841
Si2	0.1059	0.5860	0.3843
Si3	0.1591	0.8752	0.5281
O1	0.2500	0.8750	0.0000
O2	0.1095	0.3756	0.4211
O3	0.1756	0.6301	0.3096
O4	0.1717	0.1201	0.3087
O5	0.1149	0.0542	0.4860
O6	0.1147	0.6965	0.4858
O7	0.0212	0.6276	0.3326
O8	0.0215	0.1223	0.3370
O9	0.1494	0.8759	0.6390
O10	0.1489	0.3737	0.6347

by the program XPREP (SHELXTL PCTM, 1990). The resulting space groups and final lattice parameter are summarized in Table 1, atomic coordinates for the polytypes

polytype	general	special
family	$h, k, l = 2n$	
reflection	$h + k = 2n$	
<i>M2a2bc</i>	$l = 2n$	$h, k = 2n: h + k = 4n$ $h, k \neq 2n: h + k = 2n^a$
<i>M2a2b2c</i>	$k + l = 2n$	$h, k = 2n: h + k = 4n$ $h, k \neq 2n: h + k = 2n^a$
<i>Ma2bc</i>	$h, l = 2n$	$k = 2n: h + k = 4n$ $k \neq 2n: h + k = 2n + 1^b$
<i>Ma2b2c</i>	$h = 2n,$ $k + l = 2n$	$k = 2n: h + k = 4n$ $k \neq 2n: h + k = 2n + 1^b$

Table 6. Reflection conditions for all polytypes in the common setting ($a = 34.064$, $b = 7.363$, $c = 14.023$ Å, $\alpha = \gamma = 90^\circ$, $\beta = 90.36^\circ$).

a: This is valid for a diffraction pattern of a crystal composed of both twin individuals. The twin individuals give separate reflections with $h = 4n + k$ and $h = 4n - k$ respectively.

b: $h - k = 4n + 2$ reflections are absent. These unusual reflection absences are also found for wollastonite (Mamedov, Belov 1955, 1956a,b) and are explained by the coincidence that the *y* coordinates of almost all atoms have a value very close to $(2n + 1)/8$. Only Si1, Si2, O5 and O6 have different *y* values, but the structure factors of the corresponding "absent" reflections are so low that they can not be observed in routine precession photographs.

are given in Tables 2–5.

The $F^2(hkl)$ values simulating X-ray intensities were visualized with reciprocal space plots produced by the program XPREP (SHELXTL PCTM, 1990). To compare the reciprocal space plots of the four polytypes with each other and with recorded precession photographs of a natural sample, all polytypic structures had to be brought into a common setting (matrices for this transformation are given in Table 1). The lattice parameters for this common setting are: $a = 34.064$, $b = 7.363$, $c = 14.023$ Å, $\alpha = \gamma = 90^\circ$, $\beta = 90.36^\circ$. The orientation of the cell for the common setting is the same as for the subcell but the lengths of all axes are doubled. Hence the reflections common to all polytypes in this orientation have even *hkl* values. The reflection conditions for the different polytypes due to (1) their symmetry and (2) the transformation into the common setting are given in Table 6.

The reflections on a specific layer are given in Tables 7–9 and shown in Figs. 9–12. Because the triclinic polytypes *M2a2bc* and *M2a2b2c* usually appear twinned, the reflection condition as well as the reciprocal space plot are given for a crystal composed of both twin individuals. Fig. 13 shows how the diffraction pattern of the twin individuals superimpose.

Modeling of polytypes with this geometric approach has the disadvantage that short-range distortions, characteristic of each polytype, are not picked up. Such distortions are probably responsible for the preferred occurrence and stability of certain stacking variants.

Identification of xonotlite polytypes in single-crystal X-ray photographs

Comparison of the simulated diffraction pattern (Figs. 9–12 and Tables 7–9) shows that, as expected, reciprocal layers perpendicular to \mathbf{b}^* with even *k* values are the same for all polytypes whereas layers with odd *k* values are different and therefore characteristic of each polytype. Xonotlite crystals have needle like shape with the needle axis perpendicular to \mathbf{b}^* the crystals have to be mounted with the elongated axis perpendicular to the glass

Table 7. Reflections of the ordered xonotlite polytypes in the common setting ($a = 34.064$, $b = 7.363$, $c = 14.023$ Å, $\alpha = \gamma = 90^\circ$, $\beta = 90.36^\circ$) present on layers perpendicular to \mathbf{a}^* for layers with $h = 4n$ ($0kl$ in Fig. 9–13), $h = 2n + 1$ ($1kl$ in Fig. 9–13) and $h = 4n + 2$ ($2kl$ in Fig. 9–13).

	$h = 4n$	$h = 2n + 1$	$h = 4n + 2$
family reflections	$k = 4n$ $l = 2n$	—	$k = 4n + 2$ $l = 2n$
<i>M2a2bc</i> twinned	$k = 4n$ $l = 2n$	$k = 2n + 1$ $l = 2n$	$k = 4n + 2$ $l = 2n$
<i>M2a2b2c</i> twinned	$k = 4n$ $l = 2n$	$k = 2n + 1$ $l = 2n + 1$	$k = 4n + 2$ $l = 2n$
<i>Ma2bc</i>	$k \neq 4n + 2$ $l = 2n$	—	$k \neq 4n$ $l = 2n$
<i>Ma2b2c</i>	$k \neq 4n + 2$ $k + l = 2n - 1$	—	$k \neq 4n$ $k + l = 2n + 1$

Table 8. Reflections of the ordered xonotlite polytypes in the common setting ($a = 34.064$, $b = 7.363$, $c = 14.023$ Å, $\alpha = \gamma = 90^\circ$, $\beta = 90.36^\circ$) present on layers perpendicular to \mathbf{b}^* for layers with $k = 4n$ ($h0l$ in Fig. 9–13), $k = 2n + 1$ ($h1l$ in Fig. 9–13) and $k = 4n + 2$ ($h2l$ in Fig. 9–13).

	$k = 4n$	$k = 2n + 1$	$k = 4n + 2$
family reflections	$h = 4n$ $l = 2n$	—	$h = 4n + 2$ $l = 2n$
<i>M2a2bc</i> twinned	$h = 4n$ $l = 2n$	$h = 2n + 1$ $l = 2n$	$h = 4n + 2$ $l = 2n$
<i>M2a2b2c</i> twinned	$h = 4n$ $l = 2n$	$h = 2n + 1$ $l = 2n - 1$	$h = 4n + 2$ $l = 2n$
<i>Ma2bc</i>	$h = 4n$ $l = 2n$	$h = 2n$ $l = 2n$	$h = 4n + 2$ $l = 2n$
<i>Ma2b2c</i>	$h = 4n$ $l = 2n$	$h = 2n$ $l = 2n + 1$	$h = 4n + 2$ $l = 2n$

Table 9. Reflections of the ordered xonotlite polytypes in the common setting ($a = 34.064$, $b = 7.363$, $c = 14.023$ Å, $\alpha = \gamma = 90^\circ$, $\beta = 90.36^\circ$) present on layers perpendicular to \mathbf{c}^* for layers with $l = 2n$ ($hk0$ in Fig. 9–13), $l = 2n + 1$ ($hk1$ in Fig. 9–13).

	$l = 2n$	$l = 2n + 1$
family reflections	$h + k = 4n$ $h, k = 2n$	—
<i>M2a2bc</i> twinned	for $k = 2n$: $h + k = 4n$ for $k = 2n + 1$: $h + k = 2n$	—
<i>M2a2b2c</i> twinned	$k = 2n$ $h + k = 4n$	$k = 2n + 1$ $h + k = 2n$
<i>Ma2bc</i>	for $k = 2n$: $h + k = 4n$ for $k = 2n + 1$: $h + k = 2n + 1$	—
<i>Ma2b2c</i>	$k = 2n$ $h + k = 4n$	$k = 2n + 1$ $h + k = 2n + 1$

fiber. If the crystal is mounted with its elongation parallel to the glass needle precession photographs of the following three layers are necessary to record reflections which are characteristic of each polytype without mutual overlap: $0kl$, $hk0$, and $hk1$. The presence of the *M2a2bc* polytype is indicated by the presence of reflections with $h, k = 2n + 1$ on the $hk0$ layer. The *M2a2b2c* polytype

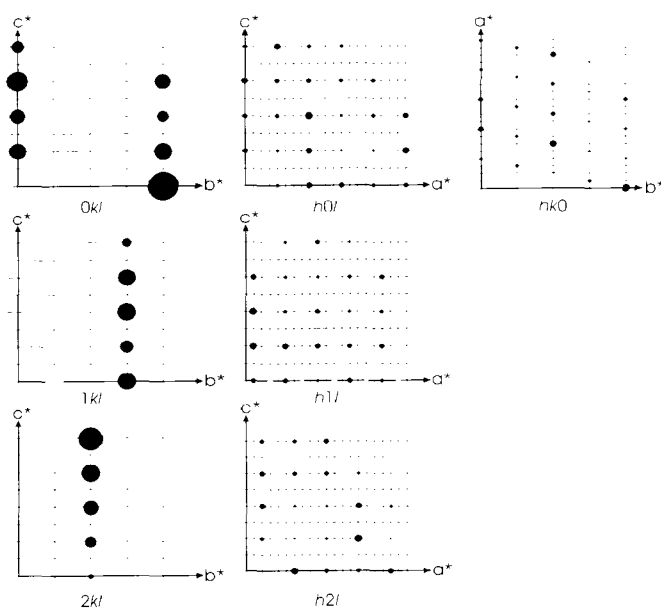


Fig. 9. Reflections of the triclinic *M2a2bc* polytype in the common setting ($a = 34.064$, $b = 7.363$, $c = 14.023$ Å, $\alpha = \gamma = 90^\circ$, $\beta = 90.36^\circ$). Black: reflections from twin component I, gray: additional reflections from twin component II. Due to arbitrary scaling for each layer, the absolute intensities in the images are not comparable between different polytypes.

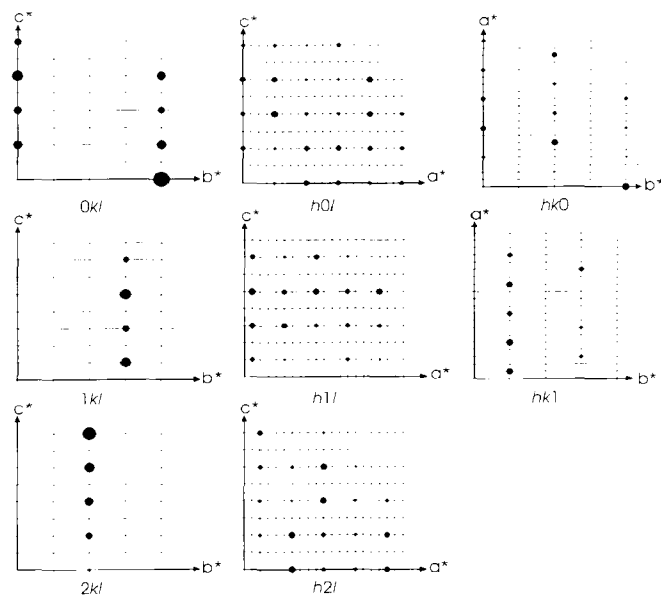


Fig. 10. Reflections of the triclinic *M2a2b2c* polytype in the common setting ($a = 34.064$, $b = 7.363$, $c = 14.023$ Å, $\alpha = \gamma = 90^\circ$, $\beta = 90.36^\circ$). Black: reflections from twin component I, gray: additional reflections from twin component II. Due to arbitrary scaling for each layer, the absolute intensities in the images are not comparable between different polytypes.

can be identified by the presence of reflections with $h, k = 2n + 1$ on the $hk1$ layer. The *Ma2bc* polytype can be resolved on the $0kl$ layer, where $k = 2n + 1$ with $l = 2n$ reflections are observed. On the same layer the *Ma2b2c* polytype has $k = 2n + 1$ with $l = 2n + 1$ reflections. All reflections conditions are related to the common setting.

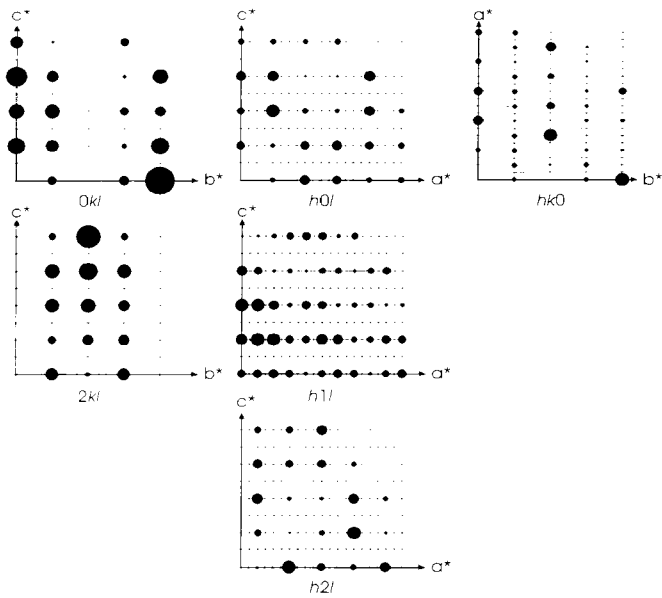


Fig. 11. Reflections of the monoclinic *Ma2bc* polytype in the common setting ($a = 34.064$, $b = 7.363$, $c = 14.023$ Å, $\alpha = \gamma = 90^\circ$, $\beta = 90.36^\circ$). Due to arbitrary scaling for each layer, the absolute intensities in the images are not comparable between different polytypes.

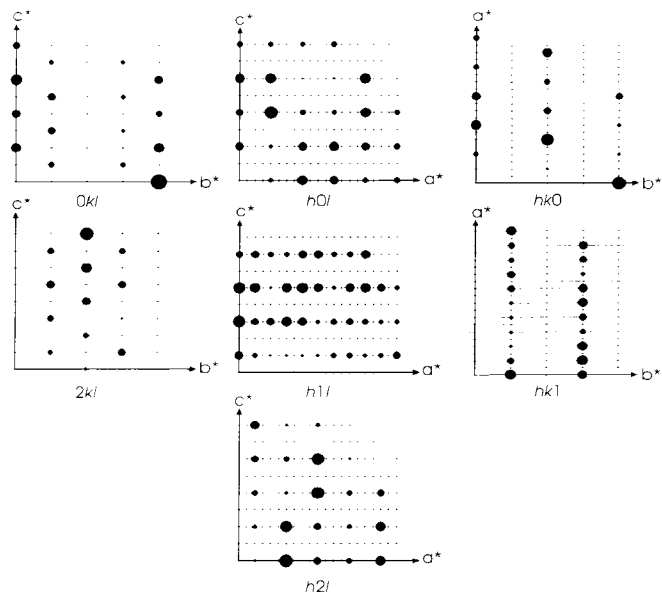


Fig. 12. Reflections of the monoclinic *Ma2b2c* polytype in the common setting ($a = 34.064$, $b = 7.363$, $c = 14.023$ Å, $\alpha = \gamma = 90^\circ$, $\beta = 90.36^\circ$). Due to arbitrary scaling for each layer, the absolute intensities in the images are not comparable between different polytypes.

Polytypism in xonotlite from the N'chwaning II mine

Crystals from the N'chwaning II mine, Kalahari Manganese Field, South Africa were mounted with \mathbf{b}^* parallel to the glass fiber to record normal-beam Weissenberg-photographs ($h0l$, $h1l$, $h2l$) and precession-photographs ($0kl$, $1kl$, $2kl$, $hk0$, $hk1$, $hk2$) using Ni-filtered $\text{CuK}\alpha$ -radiation. The lattice parameter for the common setting were found

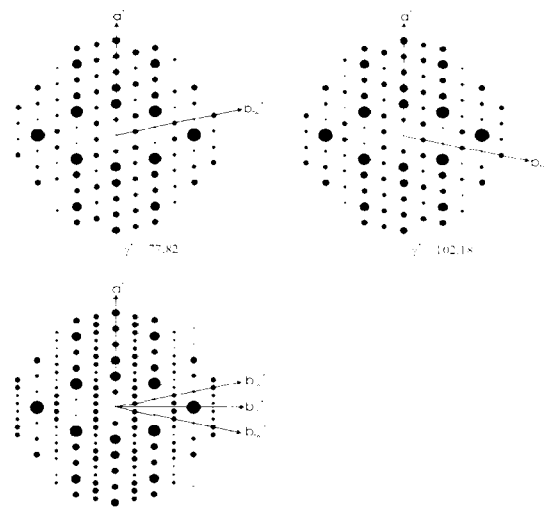


Fig. 13. Calculated diffraction pattern of the $hk0$ layer of the twin component I (upper left) and II (upper right) of the xonotlite-*M2a2bc* polytype. Bottom picture shows the diffraction pattern of the two twin components together.

to be $a = 33.76$, $b = 7.38$, $c = 13.82$ Å, $\alpha = \beta = \gamma = 90^\circ$. The recorded reflections of one crystal on precession-photographs and their assignment to polytypes are listed in Tables 10 and 11, two exemplary details of the precession-photographs of one crystal are shown in Figs. 14 and 15. If the common strong family reflections are ignored, the strongest of the remaining reflections can be assigned to a twin component of the *M2a2b2c* polytype. The second twin component and the *Ma2b2c* polytype give reflections of intermediate intensity. Remaining weak reflections can be assigned to the *Ma2bc* polytype. Reflections characteristic of the *M2a2bc* polytype were not observed.

Pronounced streaks were found parallel to \mathbf{a}^* at $k = 2n + 1$ for even and odd l and faint streaks parallel to \mathbf{c}^* at $k = 2n + 1$ for even and odd h . Thus, not only domains of ordered but also domains of disordered polytypes

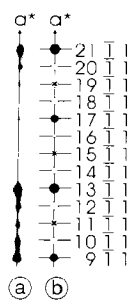


Fig. 14. (a) Detailed view of recorded $h\bar{1}l$ reflections on a precession-photograph (Ni-filtered $\text{CuK}\alpha$ -radiation) of xonotlite. (b) Calculated $h\bar{1}l$ reflections (common setting $a = 34.064$, $b = 7.363$, $c = 14.023$ Å, $\alpha = \gamma = 90^\circ$, $\beta = 90.36^\circ$) for the *M2a2b2c* xonotlite polytype (full circles for twin component I and dark gray spots with cross for twin component II) and for the *Ma2b2c* xonotlite polytype (empty circles). Both twin components of the *M2a2b2c* polytype ($h = 4n + 1$ for twin component I and $h = 4n - 1$ for twin component II) and the monoclinic *Ma2b2c* polytype ($h = 2n$) contribute to the observed $h\bar{1}l$ reflections. $h\bar{1}l$ reflections are overlaid by pronounced streaks, running parallel to \mathbf{a}^* at $k = -1$. Note that the streak intensity is modulated and the modulation is in correlation with the intensity of the Bragg reflections.

Table 10. Recorded reflections of a xonotlite sample from N'chwaning II on layers perpendicular to \mathbf{a}^* .

layer perpendicular to \mathbf{a}^*	reflections present for	relative intensity	possible polytype
$h = 4n$	$k = 4n: l = 2n + 1$	s	<i>Ma2b2c</i>
	$k = 4n: l = 2n$	w	<i>M2a2b2c</i>
$h = 2n + 1$	$k = 4n + 1: l = 2n - 1$	s	<i>M2a2b2c</i>
	$k = 4n + 1: l = 2n$	w	<i>Ma2bc</i>
$h = 4n + 2$	$k = 4n + 2: l = 2n + 1$	s	<i>Ma2b2c</i>
	$k = 4n + 2: l = 2n$	w	<i>Ma2bc</i>

s strong reflections
w weak reflections

Table 11. Recorded reflections of a xonotlite sample from N'chwaning II on layers perpendicular to \mathbf{c}^* .

layer perpendicular to \mathbf{c}^*	reflections present for	relative intensity	possible polytype
$l = 2n$	$k = 2n: h = k = 4n$	s	<i>M2a2b2c, Ma2b2c</i>
	$k = 2n - 1: h = 4n - 1$	s	<i>M2a2b2c</i> (tw1)
$l = 2n + 1$	$k = 2n + 1: h = 4n - 1$	w	<i>M2a2b2c</i> (twII)
	$k = 2n + 1: h = 2n + 1$	w	<i>Ma2b2c</i>

s strong reflections
w weak reflections

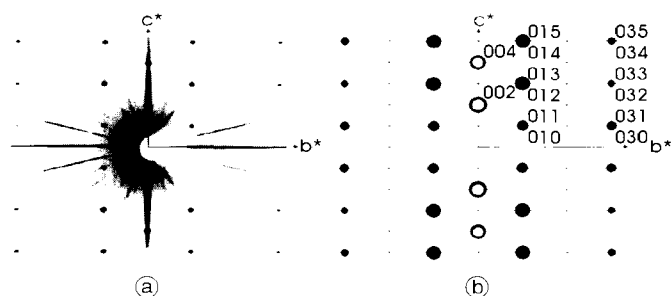


Fig. 15. (a) Recorded precession-photograph (Ni-filtered $\text{CuK}\alpha$ -radiation) of the $0kl$ layer of xonotlite. (b) Calculated $0kl$ reflections (common setting: $a = 34.064$, $b = 7.363$, $c = 14.023$ Å, $\alpha = \gamma = 90$, $\beta = 90.36^\circ$) for the *Ma2b2c* (black spots) and the *Ma2bc* (gray spots) xonotlite polytypes, coinciding reflections are gray with black rims. Strong reflections with $k + l = 2n$ can be assigned to the monoclinic *Ma2b2c* polytype and weak reflections with $l = 2n$ to the monoclinic *Ma2bc* polytype. For $k = 4n$ the reflections of all polytypes coincide, for $h - k = 4n - 2$ the reflections of all polytypes are absent. Faint streaks are visible parallel to \mathbf{c}^* at $k = 2n + 1$. Radial streaks are caused by white radiation.

are present. The intensities of the streaks are not constant but modulated. The intensity modulation of the streaks is correlated with the intensity of the sharp Bragg reflections from the individual polytypes. The absence of additional diffuse intensity maxima within the streaks leads to the suggestion that no correlation between sequences of polytype domains are present.

The higher-level Weissenberg-photographs have been recorded in normal-beam camera-setting (without rotating the camera as in an equi-inclination camera setting; X-ray beam perpendicular to the camera). After the photographs were scanned, the reflection coordinates were reconstructed to reciprocal space coordinates with the program dwb99 (Weber, 1999). Fig. 16 shows the rectified image of the hll layer recorded by normal-beam Weissenberg-technique. In general, such rectified Weissenberg-photographs have two advantages over precession-photographs displaying corresponding reciprocal lattices. (1) In the

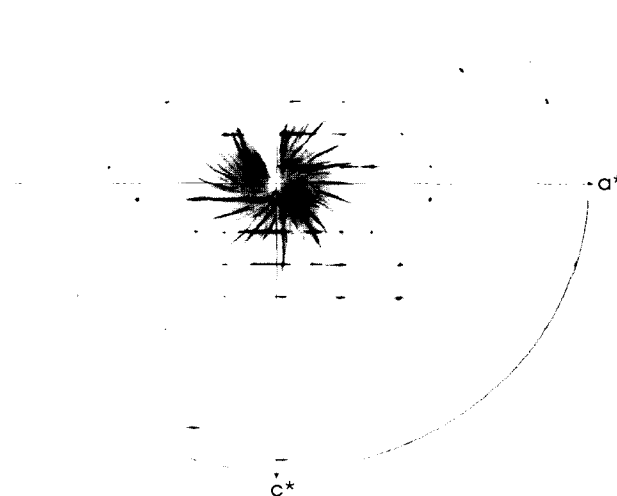


Fig. 16. Recorded normal-beam Weissenberg-photograph (Ni-filtered $\text{CuK}\alpha$ -radiation) of the hll layer of xonotlite (common setting: $a = 34.064$, $b = 7.363$, $c = 14.023$ Å, $\alpha = \gamma = 90$, $\beta = 90.36^\circ$). Streaks and reflections are present for $l = 2n + 1$, such reflections are present for the *M2a2b2c* and the *Ma2b2c* xonotlite polytype. Reflections for $h = 4n + 1$ can be assigned to one twin component of the *M2a2b2c* polytype, reflections for $h = 4n - 1$ and for $h = 2n$ are visible on the original photograph but can not be resolved within the streaks on the rectified picture. Reflections for $l = 2n$ and $h = 2n$ are very weak and hardly visible on the rectified picture. Although precession photographs perpendicular to \mathbf{a}^* of the same crystal showed streaks parallel to \mathbf{c}^* these streaks are too weak to be reproduced.

Weissenberg-technique there is no blind spot for low θ reflections as caused by the layer screen for higher-level precession-photographs. (2) For strongly streaked reflections along \mathbf{a}^* and \mathbf{c}^* of fibrous (parallel to \mathbf{b}) crystals, it is rather difficult to obtain a good crystal orientation ($h0l$) by the precession-method whereas sharp rotation-photographs along \mathbf{b}^* can easily be achieved. With the knowledge obtained from precession photographs of the same crystal, reflections are expected for three ordered polytypes and streaks for the disordered polytypes. However,

only reflections for one twin component of the *M2a2b2c* polytype can be resolved and streaks parallel to \mathbf{a}^* for odd l are visible (Fig. 16). The reason is the strong streaking parallel to \mathbf{a}^* and the moderate streaking parallel to \mathbf{c}^* in xonotlite. Thus a recorded $h1l$ reciprocal space image represents the maximum diffuseness for all reflections. In this orientation the contrast between reflection intensity and background is only poorly defined. This example demonstrates that it is more suitable to record photographs of the $0kl$, $hk0$, and $hk1$ layers for identification of ordered and disordered xonotlite polytypes than a photograph of the $h1l$ layer.

Further investigations on other xonotlite crystals from the same locality gave similar results. The *M2a2b2c* polytype was in all cases the dominant polytype although with varying degree of twinning, followed by the *Ma2b2c* polytype and traces of the *Ma2bc* polytype.

As mentioned in the structure description of xonotlite, OH groups are located on the free apices of calcium octahedra where no bridging SiO_4 tetrahedra are attached. In the *M2a2bc* and *Ma2bc* polytypes half of the CaO_6 octahedra have two OH groups attached and the other half has no OH groups but instead bonds to two SiO_4 tetrahedra (Fig. 5). In the *M2a2b2c* and *Ma2b2c* polytypes each CaO_6 octahedron carries one OH group. This latter OH distribution is more balanced and seems therefore more favorable. Thus *M2a2b2c* and *Ma2b2c* are expected to occur more often. This is also partly confirmed by Chisholm's investigations (1980). He found the *Ma2b2c* polytype to be the most frequent one, followed by the *Ma2bc* polytype, and the *M2a2b2c* polytype was only detected as small regions within the *Ma2b2c* polytype. The *M2a2bc* polytype has never been found. The dominant occurrence of the *M2a2b2c* polytype reported by Kudoh and Takéuchi (1979) and in the crystals from the N'chwaning II mine, however, leads to the suggestion that other so far not understood reasons favor this polytype in the two investigated samples.

OD approach

Structural relations between xonotlite and related C–S–H minerals

Comparison of the structures of wollastonite CaSiO_3 , clinotobermorite $\text{Ca}_5\text{Si}_6\text{O}_{17} \cdot 5 \text{H}_2\text{O}$, 9 Å-tobermorite $\text{Ca}_5\text{Si}_6\text{O}_{16}(\text{OH})_2$, 11 Å-tobermorite $\text{Ca}_{4-x}\text{Si}_6\text{O}_{15-2x}(\text{OH})_{2-2x} \cdot 5 \text{H}_2\text{O}$, 14 Å-tobermorite $\text{Ca}_5\text{Si}_6\text{O}_8(\text{OH})_2 \cdot 8 \text{H}_2\text{O}$, and foshagite $\text{Ca}_4\text{Si}_3\text{O}_9(\text{OH})_2$, shows that they are in some respect similar to xonotlite. All of them consist of calcium polyhedral layers or ribbons characteristic of the mineral and its polytypes, and single or double chains of SiO_4 tetrahedra. The chains of SiO_4 tetrahedra have a periodicity of three tetrahedra and a length of $b = 7.3 \text{ \AA}$. The edges of two calcium polyhedra have about the same length as a chain fragment composed of three SiO_4 tetrahedra (Fig. 3). In the substructure with halved \mathbf{b} translation ($b/2 = 3.66 \text{ \AA}$) the chains of tetrahedra are therefore superimposed. The diffraction patterns of the above structures show comparable features as both sharp and diffuse

reflections, diffuse streaks, and a strong pseudo-translation of $\mathbf{b}/2$. Furthermore, they appear as different polytypes.

The two wollastonite polytypes, wollastonite-1A and wollastonite-2M (Trojer, 1968; Peacor, Prewitt, 1963) as well as polytypes of 9 Å-tobermorite, 11 Å-tobermorite and clinotobermorite (Merlino, Bonaccorsi, Armbruster, 1999, 2000; Hoffmann, Armbruster, 1997) have been interpreted in terms of OD-theory (Dornberger-Schiff, 1956, 1964; Merlino, 1997). Their structures are looked upon as OD-structures built up by equivalent layers (Merlino, 1997, Merlino et al., 1999, 2000). These equivalent layers are called OD-layers and are not always identical to crystallochemical layers (Grell, 1984). The OD-layers are characteristic of a family of OD-structures and common to all family members. In the different polytypic members of one OD-family the OD-layers are stacked in different ways. The symmetry of an OD-layer (described by a λ operation) as well as the coincidence operations that link OD-layers (partial symmetry operations, σ operations) have to be determined. With these two sets of operations the various polytypes can be derived. Each combination of λ - and σ operation applied to the OD-layers leads to a set of sharp reflections that is common to all members of a family of OD-polytypes. Therefore, these reflections are named family reflections and a structure based only on them is referred as family structure or subcell structure.

Considering similarities in structure and diffraction characteristics it can be concluded that xonotlite and foshagite polytypes (Gard, Taylor, 1958, 1959, 1960) can also be explained in terms of OD-theory (Dornberger-Schiff, 1964; Āurovič, 1997). However, the polytypes of wollastonite and tobermorite exhibit one-dimensional disorder in one direction, whereas the polytypes of xonotlite and foshagite show one-dimensional disorder in two directions. Accordingly the structures of xonotlite and foshagite polytypes cannot be explained with only one kind of OD-layers but with two kinds of OD-layers or, as suggested by Dornberger-Schiff (1964), with two kinds of OD-rods.

OD-character of xonotlite

Xonotlite displays one-dimensional disorder in two directions, along \mathbf{a} and along \mathbf{c} . However, *sensu strictu*, only the disorder along \mathbf{a} conforms with OD-theory. For stacking disorder along \mathbf{c} the two possible arrangements display pairs of adjacent layers which are geometrically not equivalent, thus the vicinity condition for OD-structures is not fulfilled (Dornberger-Schiff, 1964; Āurovič, 1997). This is best seen in the distribution of OH groups (Fig. 4) in the two stacking variants. For this reason two OD-groupoid families, distinct by (1) simple (for the *Ma2bc* and the *M2a2bc* polytype) and (2) doubled periodicity (for the *Ma2b2c* and the *M2a2b2c* polytype) parallel to \mathbf{c} are defined. The corresponding OD-layers are very similar to that in wollastonite (Merlino, 1997). They are defined by the translation periods \mathbf{b} , \mathbf{c} , and a third basis vector \mathbf{a}_0 which is not a translational vector. For the polytypes with simple periodicity parallel to \mathbf{c} (Fig. 17) this is $a_0 = 8.516$, $b = 7.363$, $c = 7.012 \text{ \AA}$, $\alpha = \gamma = 90^\circ$, $\beta = 90.36^\circ$ of $P(1)2/m1$ symmetry (λ operation) and for polytypes with doubled periodicity parallel to \mathbf{c} it is $a_0 = 8.516$, $b = 7.363$,

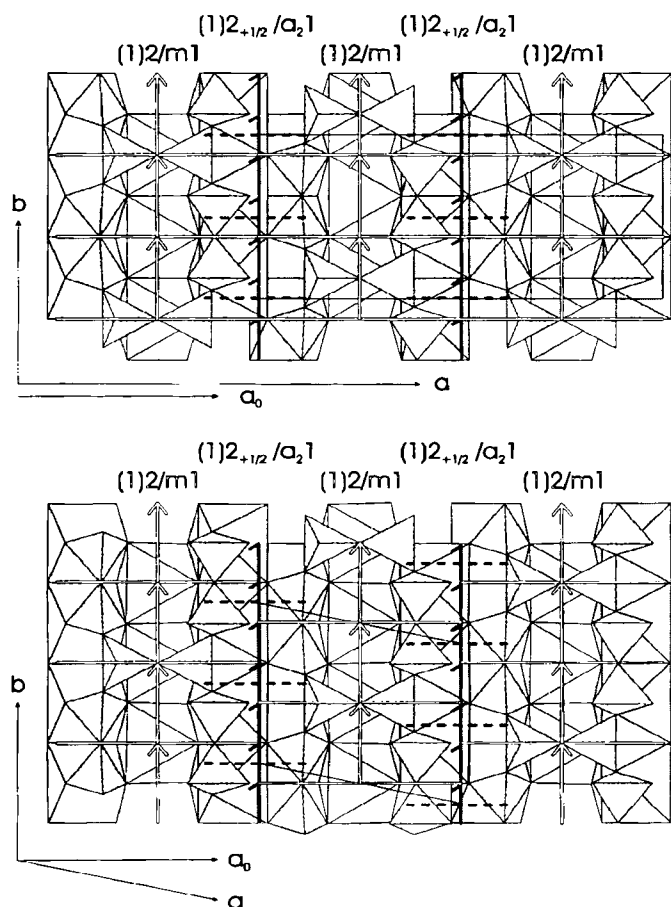


Fig. 17. Xonotlite- $M2a2bc$ and xonotlite- $Ma2bc$ in terms of OD-theory. Solid out-lines of the true cell are given. Symmetry operations (λ operations) of the OD-layers ($2/m$) are drawn in white with black rim, partial symmetry operations (σ operations) relating adjacent OD-layers ($2_{1/2}a_2$) in black.

$c = 14.023 \text{ \AA}$, $\alpha = \gamma = 90$, $\beta = 90.36^\circ$ of $A(1)2/m1$ symmetry (λ operation). The partial symmetry operation (σ operation) that relates pairs of adjacent layers is a two-fold screw axis with a translational component of $+b/4$ or $-b/4$ (instead of conventional $b/2$), labeled $2_{1/2}$ or $2_{-1/2}$, and a glide normal to this two-fold screw axis with a translation component of a_0 (instead of conventional $a/2$), labeled a_2 . The σ operation that describes the relation between adjacent layers is therefore $2_{1/2}a_2$. Different sequences of operators $2_{1/2}$ and $2_{-1/2}$ give rise to different structures. An infinite number of polytypes or disordered structures is possible depending on the ordered or disordered sequence of $2_{1/2}$ and $2_{-1/2}$ operators. A regular alternation of $2_{1/2}a_2$ and $2_{-1/2}a_2$ operators brings the first OD-layer to the same level as the third one and makes the 2_1 screw axis of the single layer valid for the whole structure. The a_2 glide plane relating adjacent layers can also be continued and becomes valid for the whole structure. Thus the alternate operations of $2_{1/2}a_2$ and $2_{-1/2}a_2$ between pairs of adjacent OD-layers with simple periodicity along c yields the $Ma2bc$ polytype of $P2/a$ symmetry, and with doubled periodicity along c yields the $M2a2bc$ polytype of $A2/a$ symmetry. In terms of OD-theory these are polytypes with maximum degree of order named MDO₂ polytypes. The

derivation of MDO polytypes for xonotlite is similar to wollastonite and additional details are discussed by Merlino (1997). On the other hand, if the $2_{1/2}$ (or $2_{-1/2}$) operator is continuously applied neither the 2_1 screw axis, the mirror plane, nor the glide plane of the OD-layer are valid for the whole structure, only the inversion center remains. The resulting structures have $a = a_0$ and $P\bar{1}$ symmetry for the $M2a2bc$ polytype with simple periodicity along c and $A\bar{1}$ symmetry for the $M2a2b2c$ polytype with doubled periodicity parallel to c . Notice that a structure obtained by continuous application of $2_{1/2}$ is the same as the one obtained by continuous application $2_{-1/2}$ and both represent (100) twinned counterparts. $M2a2bc$ and $M2a2b2c$ polytypes derived by continuous application of the $2_{1/2}$ operator are classified as MDO₁ polytypes (e.g., Merlino, 1997). Thus the four MDO polytypes belong to two OD families, one consisting of primitive, the other of A-centered layers. Both families, however, have the same family structure.

In the above example the OD groupoid families of xonotlite were derived from the known structural principles. One of the major advantages of OD-theory is that the symmetry properties of OD-structures can also be derived from the diffraction pattern. A detailed example (wollastonite) is given by Merlino (1997). Knowledge of the family structure, based on the family reflections, combined with OD groupoid information allows to construct or predict real structures.

Acknowledgments. This work was supported by the Swiss National Fond. We thank S. Đurović, S. Merlino, and T. Weber for fruitful discussion, constructive suggestions and comments.

References

- Brown, P. A.: Xonotlite: a new occurrence at Rose Blanche, Newfoundland. *Can. Mineral.* **16** (1978) 671–672.
- Chisholm, J. E.: Polytypism in xonotlite, $\text{Ca}_6\text{Si}_6\text{O}_{17}(\text{OH})_2$. *Electron Microscopy and Analysis*, 1979, Inst. Phys. Conf. Ser. no 52 1980: Chapter 2, 109–112.
- deBruijn, H.; Schoch, A. E.; van der Westhuizen, W. A.; Beukes, G. J.: The chemical composition of xonotlite and associated inesite from the Nchwaning and Wessels mines, Kalahari manganese field, South Africa. *N. Jb. Miner. Mh.* 1999, 212–222.
- Dent, L. S.; Taylor, H. F. W.: The dehydration of xonotlite. *Acta Crystallogr.* **9** (1956) 1002–1004.
- Dornberger-Schiff, K.: On order-disorder structures (OD-Structures). *Acta Crystallogr.* **9** (1956) 593–601.
- Dornberger-Schiff, K.: Grundzüge einer Theorie der OD-Strukturen aus Schichten. *Abhandlungen der Deutschen Akademie der Wissenschaften zu Berlin, Klasse für Chemie, Geologie und Biologie* **3** (1964) 1–107.
- Đurović, S.: Fundamentals of the OD theory. *EMU Notes in Mineralogy* **1** (1997) 3–28.
- Eberhard, E.; Hamid, S. A.; Röttger, B.: Strukturverfeinerung und Polytypie von Xonotlit $\text{Ca}_6[\text{Si}_6\text{O}_{17}](\text{OH})_2$. *Z. Kristallogr.* **154** (1981) 271–272.
- FCGEN: Program for calculation of structure factors. Laboratorium für Kristallographie, Universität Bern, Schweiz, 1998.
- Gard, J. A.: A system of nomenclature for the fibrous calcium silicates, and a study of xonotlite polytypes. *Nature* **211** (1966) 1078–1079.
- Gard, J. A.; Taylor, H. F. W.: Foshagite: composition, unit cell and dehydration. *Am. Mineral.* **43** (1958) 1–15.
- Gard, J. A.; Taylor, H. F. W.: Crystal structure of foshagite $\text{Ca}_4\text{Si}_3\text{O}_9(\text{OH})_2$. *Nature* **183** (1959) 171–173.
- Gard, J. A.; Taylor, H. F. W.: The crystal structure of foshagite. *Acta Crystallogr.* **13** (1960) 785–793.

- Grell, H.: How to choose OD layers. *Acta Crystallogr.* **A40** (1984) 95–99.
- Grimmer, A. R.; Wieker, W.: Bestimmung der Art der Wasserbindung in Xonotlit $6\text{CaO} \cdot 6\text{SiO}_2 \cdot \text{H}_2\text{O}$. *Z. anorg. allg. Chem.* **384** (1971) 34–42.
- Guinier, A.; Bokij, G. B.; Boll-Dornberger, K.; Cowley, J. M.; Đurovič, S.; Jagodzinski, H.; Krishna, P.; DeWolff, P. M.; Zvyagin, B. B.; Cox, D. E.; Goodman, P.; Hahn, Th.; Kuchitsu, K.; Abrahams, S. C.: Nomenclature of polytype structures. Report of the International Union of Crystallography Ad-Hoc Committee on the Nomenclature of Disordered, Modulated and Polytype Structures. *Acta Crystallogr.* **A40** (1984) 399–404.
- Hoffmann, C.; Armbruster, T.: Clinotobermorite, $\text{Ca}_5[\text{Si}_3\text{O}_8(\text{OH})]_2 \cdot 4\text{H}_2\text{O}$ $\text{Ca}_5[\text{Si}_6\text{O}_{17}] \cdot 5\text{H}_2\text{O}$, a natural C–S–H(I) type cement mineral: determination of the substructure. *Z. Kristallogr.* **212** (1997) 864–873.
- Kalousek, G. L.; Roy, R.: Crystal chemistry of hydrous calcium silicates: II. characterization of interlayer water. *J. Amer. Ceram. Soc.* **40** (1957) 236–239.
- Kalousek, G. L.; Mitsuda, T.; Taylor, H. F. W.: Xonotlite: cell parameters, thermogravimetry and analytical electron microscopy. *Cem. Concr. Res.* **7** (1977) 305–312.
- Kaye, C. A.: A xonotlite occurrence in Puerto Rico. *Am. Mineral.* **38** (1953) 860–862.
- Komarneni, S.; Roy, R.; Roy, D. M.: Pseudomorphism in xonotlite and tobermorite with Co^{2+} and Ni^{2+} exchange for Ca^{2+} at 25 °C. *Cem. Concr. Res.* **16** (1985) 47–58.
- Kudoh, Y.; Takéuchi, Y.: Polytypism of Xonotlite: (I) structure of an A1 polytype. *Mineral. J.* **9** (1979) 349–373.
- Larsen, E. S.: The identity of eakleite and xonotlite. *Am. Mineral.* **8** (1923) 181–182.
- Libowitzky, E.: Correlation of O–H stretching frequencies and O–H...O hydrogen bond lengths in minerals. *Monatsh. Chem.* **130/8** (1999) 1047–1059.
- Majer, V.; Barić, L.: Xonotlit und Pektolith aus basischen Gesteinen des Peridotitgabbrokomplexes im Zlatibor-Gebirge, Jugoslawien. *Tschermak's Mineral. u. Petr. Mitt.* **15** (1971) 43–55.
- Mamedov, Kh. S.; Belov, N. V.: Crystal structure of xonotlite (Kristallicheskaia structura ksonotlita). *Dokl. Akad. Nauk SSSR* **104** (1955) 615–618.
- Mamedov, Kh. S.; Belov, N. V.: Crystal structures of the mineral group wollastonite. I. structure of xonotlite (Kristallicheskaia structura mineralow gruppilji wollastonita. I. structura ksonotlita). *Zapiskii Vsesoyuz. Miner. Obschest* **85** (1956a) 13–38.
- Mamedov, Kh. S.; Belov, N. V.: Crystal structure of wollastonite (Kristallicheskaia structura wollastonita). *Dokl. Akad. Nauk SSSR* **107** (1956b) 463–466.
- McCulloch, C. E.; Angus, M. J.; Crawford, R. W.; Rahman, A. A.; Glasser, F. P.: Cements in radioactive waste disposal: some mineralogical considerations. *Mineral. Mag.* **49** (1985) 211–221.
- Merlino, S.: OD approach in minerals: examples and applications. *EMU Notes in Mineralogy* **1** (1997) 29–54.
- Merlino, S.; Bonaccorsi, E.; Armbruster, T.: Tobermorite-group minerals: crystal structures, OD features, thermal behaviour. *Am. Mineral.* **84** (1999) 1613–1621.
- Merlino, S.; Bonaccorsi, E.; Armbruster, T.: The real structure of clinotobermorite and tobermorite 9A: OD character, polytypes and structural relationships. *Eur. J. Mineral.* **12** (2000) 411–429.
- Noma, H.; Adachi, Y.; Matsuda, Y.; Yokoyama, T.: ^{29}Si and ^1H NMR of natural and synthetic xonotlite. *Chem. Lett.* 1998, 219–220.
- O'Brien, J. P.; Rodgers, K. A.: Xonotlite and rodingite from Waire, New Zealand. *Mineral. Mag.* **39** (1973) 233–240.
- Peacor, D. R.; Prewitt, C. T.: Comparison of the crystal structure of bustamite and wollastonite. *Am. Mineral.* **48** (1963) 588–596.
- Prodan, A.; Marinković, V.; Vene, N.; Kurbus, B.; Boswell, F. W.: On structural relations between the $\text{CaO}-\text{SiO}_2-\text{H}_2\text{O}$ phases. *Z. Kristallogr.* **164** (1983) 189–209.
- Rammelsberg, C.: Über den Xonotlit, ein neues wasserhaltiges Kalksilikat, und den Bustamit aus Mexiko. *Z. deut. geol. Ges.* **18** (1866) 33–34.
- SHELXTL PCTM, Release 4.1. Siemens Analytical X-Ray Instruments, Inc., Madison, WI 53719, USA 1990.
- Shrivastava, O. P.; Komarneni, S.; Breval, E.: Mg^{2+} uptake by synthetic tobermorite and xonotlite. *Cem. Concr. Res.* **21** (1991) 83–90.
- Smith, C. H.: On the occurrence and origin of xonotlite. *Am. Mineral.* **39** (1954) 531–532.
- Stuckemeier, I.; Dettmann, P.; Mangold, K.; Schweers, H.: Similitude theory considerations in the production of calcium hydrosilicates from lime-rich mixtures. *Zement Kalk Gips Internat.* **52(5)** (1999) 264–272.
- Taylor, H. F. W.: The identity of jurupaite and xonotlite. *Mineral. Mag.* **30** (1954) 338–341.
- Taylor, H. F. W.: The transformation of tobermorite into xonotlite. *Mineral. Mag.* **32** (1959) 110–116.
- Taylor, H. F. W.: *Cement chemistry*, 2nd edition, Thomas Telford, London, 1997.
- Trojer, F.: The crystal structure of parawollastonite. *Z. Kristallogr.* **127** (1968) 291–308.
- Weber, T.: dwb99. Programm to rectify Weissenberg-photographs to reciprocal space coordinates. Laboratorium für Kristallographie, Universität Bern, Schweiz, 1999.
- Yanagisawa, K.; Feng, Q.; Yamasaki, N.: Hydrothermal synthesis of xonotlite whiskers by ion diffusion. *J. Mater. Sci. Lett.* **16** (1997) 889–891.